Evaluation of SnS:Cu Thin Film Properties Obtained by USP Technique to Implement It as an Absorbent Layer in Solar Cells Using SCAPS

Sergio Rodríguez-Castro [1], Carlos Álvarez-Macías [1,*] , Michel Rivero [2] , Lizbeth Salgado-Conrado [3], Rodrigo Loera-Palomo [4] , Bernardo Reyes-Durán [1] and Jorge Narro-Ríos [5]

[1] Tecnológico Nacional de México/Instituto Tecnológico de la Laguna, Torreón 27000, Coahuila, Mexico; sergio_RC18@hotmail.com (S.R.-C.); bernardoreydu@gmail.com (B.R.-D.)
[2] Instituto de Investigaciones en Materiales, Unidad Morelia–UNAM, Morelia 58190, Michoacán, Mexico; mrivero@materiales.unam.mx
[3] Facultad de Ingeniería Mecánica y Eléctrica, Universidad Autónoma de Coahuila, Torreón 27276, Coahuila, Mexico; lizbeth_salgado@uadec.edu.mx
[4] CONACYT-TecNM/Instituto Tecnológico de la Laguna, Torreón 27000, Coahuila, Mexico; rloerap@correo.itlalaguna.edu.mx
[5] UNAM/Instituto de Energías Renovables, Cuernavaca 62580, Morelos, Mexico; jsnar@ier.unam.mx
* Correspondence: calvarezm@correo.itlalaguna.edu.mx

Abstract: Tin sulfide doped with copper (SnS:Cu) thin films were deposited on glass substrates by the ultrasonic spray pyrolysis (USP) technique at different concentration ratios (y = [Cu]/[Sn] = 0% (undoped), 2%, 5% and 10%). The aim of this work is to analyze the effect of copper on structural, morphological, and optoelectronic properties of SnS:Cu and discuss their possible application as an absorber layer in a solar cell structure proposed which is simulated using SCAPS software. X-ray diffraction (XRD) reveals an orthorhombic structure in the undoped sample and a cubic structure in doped ones. Raman spectroscopy suggests a possible unit cell size change due to the addition of Cu. Scanning electron microscopy (SEM) shows growth in grain density with an increasing y. Image analysis based on second-order features was used to discuss grain distribution. UV-VIS spectroscopy helps to find an increase of bandgap for the doped samples when copper concentration increases, going from 1.82 eV in the doped film y = 2% to 2.2 eV in the 10% doped samples. A value of 3.51 eV was found for the undoped sample y = 0%. A rise in both carrier concentration and mobility but a decrease in resistivity when y is increased was observed through the Hall–Van der Pauw technique. Simulations by SCAPS helped conclude that considering the material thickness, the SnS:Cu compound can be an alternative for implementation in the manufacturing of solar cells as an absorber layer since it is possible to obtain the optoelectronic properties necessary using the UPS economical technique.

Keywords: tin sulfide doped with copper; ultrasonic spray pyrolysis; SCAPS

1. Introduction

For over a century, the investigation of new advanced materials applied to the photovoltaic sector has been an object of study. These materials need to exhibit specific properties to be used in optoelectronic devices such as solar cells. For many decades, semiconductors like Si or CdTe have shown great efficiency resulting in the production of commercial modules of these types of materials. However, the production of crystalline Si can be expensive, while the toxicity of CdTe represents a disadvantage itself [1].

Recently, semiconductors belonging to the IV-VI group of the periodic table have attracted attention due to their potential use in optical applications. In particular, tin sulfide (SnS) is a binary semiconductor belonging to this group, and it is widely used

in optoelectronics and sensors devices [2], and has also been a study to use SnS for anti-corrosion applications [3]. The SnS compound is ecologically friendly, has stability due to its chemically inert surface without dangling bonds and its constituent elements are earth-abundant [2]. SnS presents a p-type electrical conductivity, a high absorption coefficient ($>10^4$ cm^{-1}), and depending on the growth technique and stoichiometry, the indirect bandgap of SnS varies between 1.07 and 1.25 eV, and the direct bandgap located at slightly higher energies varies between 1.30 and 1.39 eV. These properties make SnS a suitable candidate as an absorber layer in a p—n junction device.

Nevertheless, like most tin-based compounds, SnS's high resistivity could promote charge carrier recombination if implemented in a photovoltaic device. However, this inconvenience can be solved through doping, since some investigations have proved that resistivity can be modified by impurification of a higher conductivity element [4–6]. In this sense, copper has been a very useful element implemented in diverse solar cells structures, in addition to being used as contacts also has been integrated into new structures such as the CIGS (Cu(In, Ga)Se$_2$)-based solar cell, which is one of the most common PV materials used in the mass production of thin-film photovoltaic (TFPV) modules [7,8]. Following this idea, the importance of copper as a doping agent is relevant in this research since it has been considered in many investigations due to its proven usefulness [6,9,10].

There are some deposition techniques to obtain SnS thin film such as chemical bath [4,11,12], chemical solution process [13], radiofrequency sputtering [14,15], vacuum evaporation [16], and spray pyrolysis (SP) [6,17,18]. In particular, Ultrasonic Spray Pyrolysis (USP) is one of the simplest techniques due to its relatively cheap implementation, since it does not require a vacuum. Moreover, this technique can be scaled for large areas of deposition. In the USP technique, a precursor solution is atomized, then with a carrier gas (e.g., nitrogen), the atomized solution is driven towards the substrate until it forms a thin film [19].

Device simulation can provide deep insight into device physics and elucidate the relationship between material properties and device performance. The virtual modeling of thin films is a valuable tool for designing and testing them under different conditions and applications into devices, reducing the cost and time associated with their experimental investigation and development [20]. There are many examples of software capable of simulating the structure of a solar cell as well as the calculation of photovoltaic parameters. Among these, the Solar Cell Capacitance Simulator software (SCAPS) stands out for this work's purposes due to the possibility to simulate homojunction and heterojunction cells formed from a defined number of layers. SCAPS, being a multilayer modeling program (capable of simulating up to seven different layers with its corresponding characteristics), also specializes in the simulation of thin-film solar cells and is characterized by being an open-source software. It was developed at the University of Gent, Belgium [21].

Several approaches have been carried out to examine the properties of SnS thin films contemplating different deposition techniques as well as variations in the procedure of the method (such as doping) to improve the properties of the material. However, to the best of our knowledge, this is the first report that reviews the properties of SnS:Cu obtained by the USP technique and applies these properties in SCAPS to simulate an absorbent layer to be used in a solar cell.

Therefore, in this work, we prepare several samples of SnS doped with Cu (SnS:Cu) at different ratio concentrations (y = 0%, 2%, 5%, and 10%) through the USP technique. The aim of this work is to analyze the effect of Cu as a dopant agent on the structural, chemical, morphological, optical, and electrical properties of SnS:Cu and verify its integration as an absorbent layer in a solar cell structure using computational simulation by SCAPS.

The structure of this work is organized as follows: The experimental method is reviewed in Section 2. In Section 3, the structural, chemical, morphological, optical, and electrical characterizations of the SnS:Cu thin films are revised. In order to test the developed SnS:Cu thin films as an absorbent layer in solar cells, in Section 3.6, numerical simulation using SCAPS software is discussed.

It should be noted this is an extended work of the manuscript presented at the 45th IEEE Photovoltaic Specialists Conference [22]. The project is significantly expanded by showing studies such as Raman spectroscopy for structural properties and EDS for chemical properties. In the same way, we added a discussion on the morphological properties of the films using image analysis. Likewise, a section corresponding to the simulation of the SnS:Cu material inside a solar cell as an absorbent layer using SCAPS is proposed.

2. Experimental Method and Simulation

2.1. Materials and Synthesis

SnS:Cu thin films were deposited on glass substrates by the USP technique. The glass substrates were previously cleaned with an ultrasonic bath method. For each sample of SnS thin film, precursor solutions were prepared at 0.1 M. For non-doped SnS ($y = $ [Cu]/[Sn] = 0%) thin film deposition, Sn (II) chloride di-hydrate ($SnCl_2 \cdot 2H_2O$) precursor was dissolved in deionized water and the N, N'-Dimethylthiourea ($C_3H_8N_2S$) precursor was dissolved in a methanol (99% purity) solution. For doped SnS thin film deposition, both precursors were prepared at the same conditions, and also the dopant precursor Cu (II) chloride di-hydrate ($CuCl_2 \cdot 2H_2O$) was dissolved in deionized water and mixed in $y = $ 2%, 5%, and 10% concentrations. A YUE HUA ultrasonic nebulizer (Guangdong Yuehua Medical Apparatus Factory Co., Ltd., Shantou, China) WH-802 model with an ultrasonic frequency of 1.7 MHz was used for atomizing the precursor solutions. Nitrogen was used as carrier gas at a flow rate of 1.0 L/min. The substrates were placed in an Sn bed of the reactor at a deposition temperature of 370 °C. In Figure 1, a diagram of the technique is illustrated.
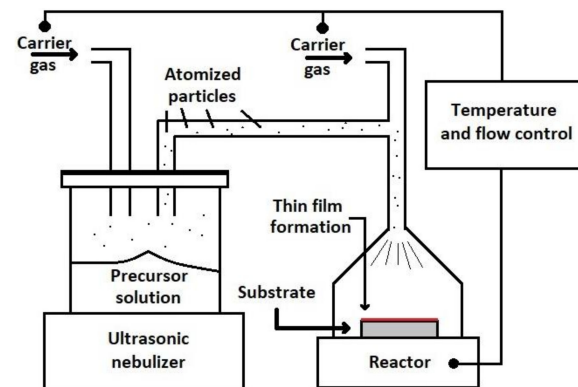
Figure 1. Diagram of USP technique.

2.2. Characterization Techniques

The structural properties of the samples were studied by the XRD technique using a Rigaku Ultima IV diffractometer (monochromatic Cu Kα radiation, λ = 0.15406 nm, Rigaku Co., Tokyo, Japan) where the 2θ angle range was varied from 20° to 60° in steps of 0.06°. Micrographs were obtained by a JEOL scanning electron microscope. The Raman spectroscopy measurement was performed with a HORIBA Jobin Yvan system (HORIBA Scientific, Kyoto, Japan) with a He-Ne laser (632 nm) at room temperature. The XFlash Detector 610 M (Bruker Co., Billerica, MA, USA) and the UV-Vis JASCO V-670 spectrophotometer (JASCO International Co., Tokyo, Japan) were used to determine the chemical composition by energy-dispersive spectroscopy (EDS), and optical properties, respectively. The wavelength was set in the range of 300–1000 nm with steps of 2 nm. The thicknesses of the films were obtained by the profilometry and measured with an AMBÍOS Technology XP-200 profilometer (Ambios Techilogy Inc., Santa Cruz, CA, USA). Electrical properties were obtained by the Hall–Van der Pauw technique using a Hall–Van der Pauw controller (MMR Technology Inc., San Jose, CA, USA).

2.3. Image Analysis

A less used tool, yet powerful and easy to implement, to quantitatively retrieve information of image characteristics is image analysis. For this particular case, grain distribution is a relevant issue. In this work, the textural features (second-order features) based on the method of grey level co-occurrence matrix (GLCM) are used. Second-order measures account for the relationship between neighbor pixels in an image and have been successfully used in other areas [23]. The variables of texture features include homogeneity, correlation, contrast, and energy [24], but in the present work, only the first two were considered. The GLCM is a square matrix, where the number of columns and rows corresponds to the number of considered gray levels in the image, which in this case are 256. This matrix considers the relation between a reference pixel and its neighbor separated at a given distance (number of pixels) and in a given direction (0°, 45°, 90°, or 135°). In this work, to avoid feature dependence on direction, the average value of the textural features from all these directions is used.

2.4. Simulation by SCAPS

Numerical simulation is a useful tool to predict the effect of changes in material properties inside a device and optimize the structure of cells. The advantage of simulation is to evaluate the performance of a system, existing or proposed, under different configurations of interest, reducing the time and cost of construction and characterization. SCAPS software can be calibrated with experimental results and can be explored to design various high-efficiency solar cells with arbitrary device dimensions/design parameters [21]. There are previous investigations on simulation of solar cells based on common photovoltaic materials such as silicon (Si) or cadmium telluride (CdTe) using the SCAPS software (version 3.2.01 and version 3.3.05 respectively) [25,26], there is even a study of the simulation of tin sulfide (SnS)-based solar cell using SCAPS [27]. However, for the research presented here, the simulation of a solar cell using SCAPS (version 3.3.10) based on SnS:Cu obtained by USP as an absorbing material is not addressed. To have a visual image of the all materials in the structure that accompanies the copper-doped tin sulfide thin film, Figure 2 shows the diagram of the solar cell structure, where the parameters of the other materials are based on Minbashi et al. and Sinsermsuksakul et al. [27,28].
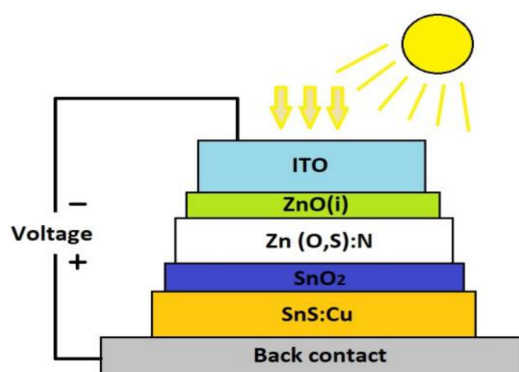
Figure 2. Structure diagram proposed to SnS:Cu thin film-based solar cell.

Indium tin oxide (ITO) serves as the window layer of the solar cell. Experimentally speaking, a thin layer of zinc oxide (ZnO) may protect the underlying layers from damage caused by the deposition of the window layer ITO [28]. Additionally, intrinsic ZnO is an attractive option in the design of transparent electrodes in thin film solar cells due to its low resistivity and simultaneous occurrence of high transmittance in the visible region [27]. Zinc oxysulfide dopped with nitrogen (Zn(O,S):N) fulfills the buffer layer role of the photovoltaic device. The material is considered with a reduced sulfur content to optimized the value of the conduction band offset, the nitrogen-doping of the material allows trapping most of the junction free electrons, restoring the rectifying quality of the

junction. It has been proved that the cell voltage can be improved through oxidation of the SnS surface resulting in a thin layer of tin dioxide (SnO_2) [28]. As mentioned, the SnS:Cu layer is intended to act as an absorbent layer inside the solar cell.

3. Results and Discussion

3.1. Structural Properties

3.1.1. X-ray Diffraction

XRD patterns of the undoped and Cu-doped SnS films are shown in Figure 3. Each diffractogram shows its correspondent copper concentration ratio y. As discussed in [22], the peak positions highlighted by the blue dashed lines in the figure found in the diffractogram of $y = 0\%$ perfectly fit a crystal lattice with an orthorhombic structure (OR) (card no. 01-071-3681). In turn, the peaks highlighted by the red dashed lines found for the diffractograms 2%, 5%, and 10% correspond to cubic crystal (CU) (card no. 01-077-3356).
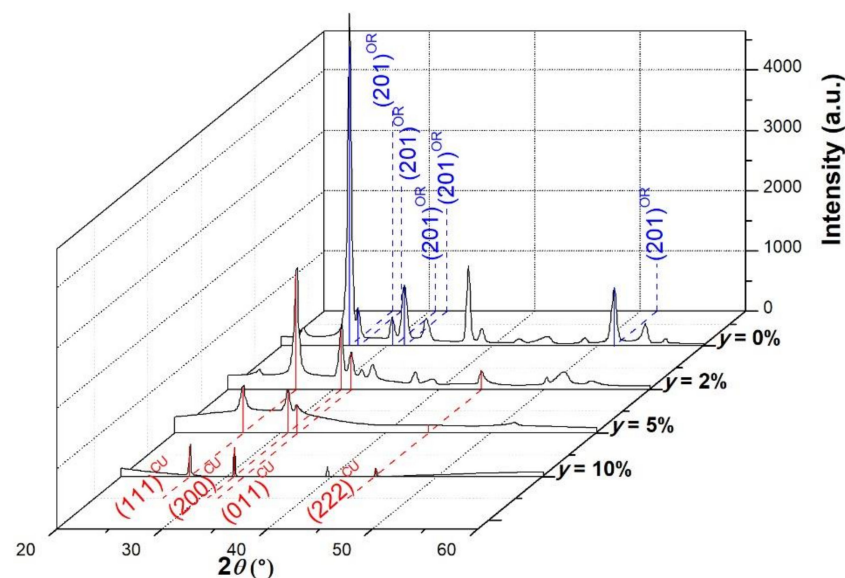
Figure 3. XRD patterns of SnS:Cu thin films at $y = 0\%$, 2%, 5%, and 10%.

The patterns in Figure 3 show that only undoped thin film has an orthorhombic crystal structure, corresponding to observed in other works [29], whereas the doped films possess a cubic structure. Other articles have also observed transitions between the CU/OR crystalline structure [30]. Besides that, it was found that increasing y causes the decreasing of the common diffraction peak located in $2\theta = 26.5°$ and the broadening of the common peak located in $2\theta = 30.5°$. These changes could indicate an increasingly amorphous behavior nature for the doped films as they increase y [22]. Namely, the crystalline state of the SnS thin films seems to be influenced by the introduction of Cu to the system. The positions of the main peaks in each crystalline structure have also been observed in other works such as in Nair et al. [31]. It can be noted that doping concentration causes a decrease in the peak intensity located in $2\theta = 26.5°$. This shows the crystalline state of the SnS:Cu thin films depends on the doping concentration y. This behavior differs from that observed when other techniques are used to synthesize the same material [10], which is an indication of the material sensitivity of this material to the synthesis procedure.

Finally, from Figure 3, it is possible to note that the peak's intensity decreases with the increase of dopant concentration. This behavior can be explained in terms of the thin thickness of the film, in which the XRD analysis is visualizing part of the glass substrate instead of the SnS:Cu, explaining the shoulders in the diffractograms of the samples with the lowest thickness.

From this study, the lattice parameters can be calculated using the Bragg law (1) and the Equations (2) and (3) for orthorhombic and cubic structures respectively [32]. The

obtained values are summarized in Table 1 along with the crystalline structure of the thin films.

$$\sin \theta = \frac{\lambda}{2\, d_{hlk}} \tag{1}$$

where θ is half the angle between the diffracted beam and the original direction of the beam, λ is the wavelength of the X-ray and d_{hkl} is the interplanar distance.

$$\frac{1}{d_{hlk}^2} = \frac{h^2}{a^2} + \frac{k^2}{b^2} + \frac{l^2}{c^2} \tag{2}$$

$$\frac{1}{d_{hlk}^2} = \frac{(h^2 + k^2 + l^2)}{a^2} \tag{3}$$

Table 1. Structural properties of Cu doped SnS thin films.

Sample	Crystalline Structure	Lattice Parameters (nm)		
		a	b	c
SnS:Cu (0%)	Orthorhombic	1.125	0.402	0.429
SnS:Cu (2%)	Cubic	0.5795	-	-
SnS:Cu (5%)	Cubic	0.5791	-	-
SnS:Cu (10%)	Cubic	0.5786	-	-

3.1.2. Raman Spectroscopy

Raman spectroscopy analysis was used to corroborate the change of crystalline structure in the deposited films. Figure 4 shows the Raman spectra obtained for the samples of SnS:Cu thin films at y = 0%, 2%, 5%, and 10%.
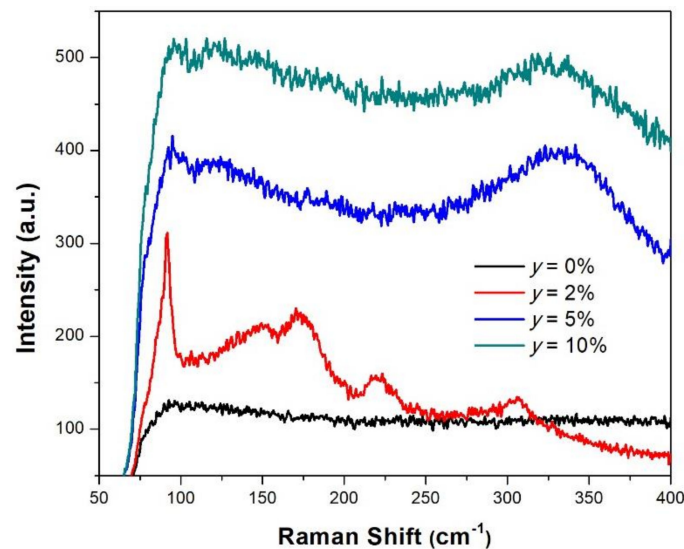
Figure 4. Raman Spectra of SnS:Cu thin films at y = 0%, 2%, 5%, and 10%.

From Figure 4, the four spectra present the main peaks characteristic of SnS. For the film y = 2%, several well-defined peaks are observed, the peaks around 95 and 218 cm^{-1} are related to the Ag vibration mode, while the peak at 170 cm^{-1} is related to the B3g vibration mode [33]. It can be noted that the peak located around 95 cm^{-1}, corresponding to the thin films y = 2%, 5%, and 10%, slightly shifts towards higher values. This may be due to the change in the size of the unit cell for the films under consideration, which could be explained by the introduction of the Cu to the unit cell in the cubic crystalline structure inducing a certain strain in the lattice [9]. It is also observed that the number of Cu atoms can vary the crystallinity, especially in y = 5% and 10%, which is also obtained

for the X-ray diffractograms. The quality of the Raman peaks is more notable for $y = 2\%$, then it decreases when y is increased to 5% and 10%, which is due to the low thickness in the films. This observation is in accordance with S. Sebastian et al. [34].

3.2. Chemical Properties

The chemical analysis of undoped and doped SnS:Cu thin films with different Cu doping concentrations was investigated by energy dispersive spectroscopy (EDS). The EDS analysis is taken in a certain area selected on the surface of each SnS:Cu thin film. The atomic percentage of these elements is given in Table 2.

Table 2. EDS results of Cu doped SnS thin films.

Samples	Atomic Percentage (%)			[Cu]/[Sn] (%)
	Sn	**S**	**Cu**	
SnS:Cu (0%)	65.44	34.56	0	0
SnS:Cu (2%)	67.41	32.37	0.22	0.32
SnS:Cu (5%)	53.77	45.74	0.49	0.91
SnS:Cu (10%)	55.13	40.69	4.18	7.58

Table 2 confirms the presence of Sn, S, and Cu elements where it is possible to observe the lack of Cu in the undoped sample while that in all doped ones is indeed present. In addition, it was observed that upon increasing the Cu concentration, the percentages of Sn and S in the film were changed. As expected, the value concentration of [Cu]/[Sn](%) is increasing as y does. This is due to the increase of Cu precursor solution when the thin films were deposited. The percentage values of this column denote that the higher the y, the greater the approximation to the proposed doping, the thin film of $y = 10\%$ being the one that is closest in proportion to this value with 7.58%, or in other words, the ratio of [Cu]/[Sn](%) to y (%) approaches unity. This can be explained by considering that the structure of the thin film begins to better absorb the doping element at a doping point greater than 5%.

3.3. Morphological Properties

Figure 5 shows the SEM images corresponding to SnS:Cu thin films with a doping concentration of $y = 2\%$, 5%, and 10%, respectively. These images were selected to implement the GLCM method for the image analysis and are different from those used at [22].
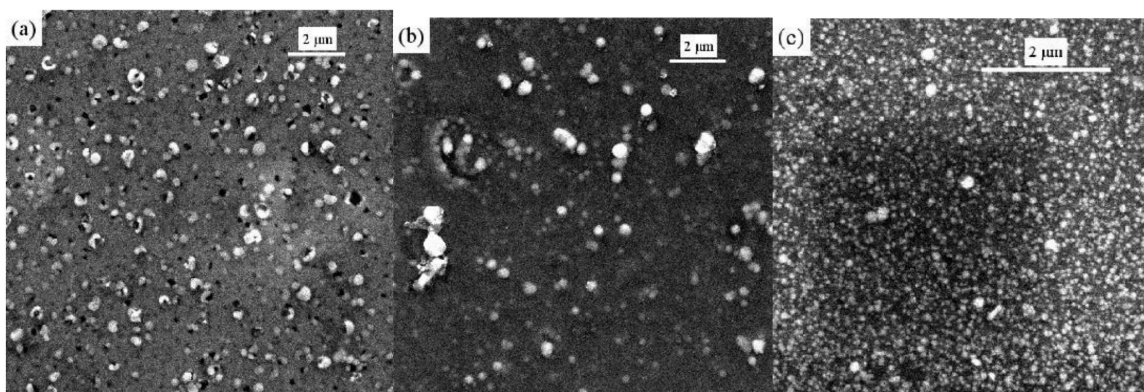
Figure 5. SEM images of the SnS:Cu thin films with doping concentration, y, of (**a**) 2%, (**b**) 5%, and (**c**) 10%.

From Figure 5, it is possible to observe that for concentrations below 5%, the film formation results in a random distribution of small crystallites (see Figure 5a,b), acting as a nucleus for further growth. The sizes of those crystals vary from 480–515 nm and 270–560 nm for 2% and 5% respectively. By increasing the concentration of Cu up to

10%, higher densification in the film is observed (Figure 5c). This can be attributed to the enhanced surface diffusion, resulting in more homogeneous distributions of the grains, which corresponds to a better distribution of the Cu element in the thin film surface with the increasing of *y*. In fact, for this concentration, crystal sizes ranged from 135–215 nm. Image analysis can be a valuable tool to quantitatively determine the uniformity in the distribution of grains over the SEM images, which is described in the next subsection.

Image Analysis Results

Table 3 shows the homogeneity and correlation for the SEM images presented in Figure 5. Homogeneity, also referred to as inverse difference moment, accounts for the uniformity of image texture distribution. High homogeneity values imply that the image is mostly at the same gray level. In fact, it can be observed that for SnS:Cu (10%) (Figure 5c) grains are more evenly distributed through all the area, resulting in a lower homogeneity value. Conversely, SnS:Cu (2%) and SnS:Cu (5%) (Figure 5a,b) present a random distribution of grains and a bigger inter-granular area, being the highest for SnS:Cu (5%) material, which is consistent with results presented in Table 3. On the other hand, correlation is a measure of the relation between the reference pixel and its neighbor, and thus reflects the consistency of image texture. In this case, the higher correlation corresponds to the SnS:Cu (10%) material, which possesses the most homogeneous distribution of grains. It is important to mention that different metrics complement each other.

Table 3. Homogeneity and correlation from images presented in Figure 5.

Sample	Homogeneity	Correlation
SnS:Cu (2%)	0.0947	0.6522
SnS:Cu (5%)	0.1023	0.7015
SnS:Cu (10%)	0.0524	0.7350

3.4. Optical Properties

Figure 6a,b show the optical transmittance and reflectance spectra respectively of thin films deposited at *y* = 0%, 2%, 5%, and 10% [22]. The absorption coefficient α was calculated for all samples, using [35]:

$$\alpha = \frac{1}{d} \ln \frac{(100 - R)}{T}, \tag{4}$$

where *d* is the film thickness, which is obtained by profilometry, *T* and *R* are the optical transmittances and reflectance respectively. Figure 6c shows the calculated α as a function of photon energy, *hv*.

From Figure 6a, an abrupt change in the absorption edge to lower wavelengths is observed in the sample at *y* = 0% (undoped) with respect to Cu-doped films. This effect may be due to the change of crystalline structure observed by the copper incorporation to the SnS system. Then the undoped sample has the highest transmission spectra in the whole range and a loss of transmittance when copper is added to the thin films in the concentration SnS:Cu, which can be due to the change of structure confirmed by the XRD and Raman measurements.

It is also possible to observe in Figure 6a that the spectrum with the minimal percent of transmittance is from the 2% doped thin film, with a shape more homogeneous dependence on the wavelength at the interval $\lambda > 400$ nm. On the other hand, shoulders to the spectra at *y* = 5% and 10% are observed, which indicates the presence of different phases in the layers [36].
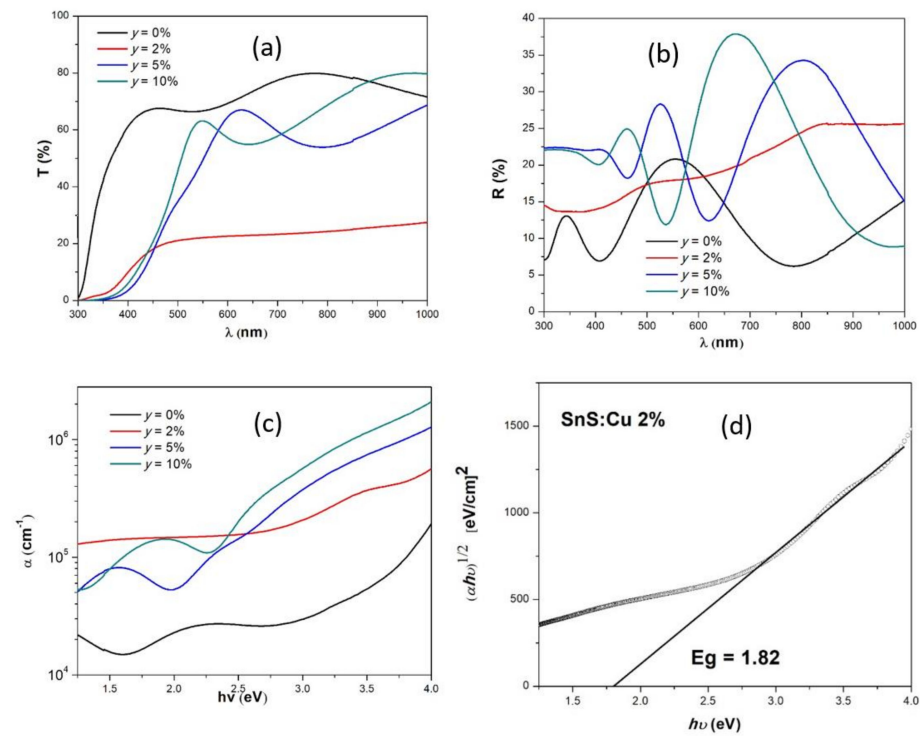
Figure 6. Transmittance (**a**) and reflectance (**b**) spectra of the SnS:Cu thin films, calculated α (**c**) and Tauc method for sample y = 2% (**d**) [22]. Copyright permission from: IEEE.

Relating to the absorption coefficient, as can be seen from Figure 6c, α increases an order of magnitude on the whole spectrum for all samples doped with Cu concerning the undoped one. It ranges from 10^4 for the lowest hv up to 10^6 for the higher hv, proving a higher value of this parameter with the increasing doping concentration. The optical band gap for the material in each sample can be estimated by applying the Tauc plotting method to the absorption coefficient α by Equation (5) [37]:

$$\alpha hv = B \left(hv - E_g\right)^{\gamma}, \tag{5}$$

where hv is the photon energy, E_g is the optical band gap, B represents a Tauc constant and γ depends on the nature of electronic transitions [37].

In this case, γ was better adjusted for the value of 2 indicating that allowed indirect optical transitions correspond to the nature of the films, which is the same proposed for the papers [11,12]. In this method, linear regression with γ = 2 is performed in the energy range where both variables present a linear dependence (high absorption region). The value of the optical band gap, E_g, corresponds to the point where the fitting line crosses the abscissa. Figure 6d represents the Tauc method applied to sample SnS:Cu (2%). Table 4 presents the values of obtained E_g for the samples SnS:Cu at y = 0%, 2%, 5%, and 10%, using the Tauc plot method for the case allowed indirect optical transitions.

Table 4. Bandgap and thickness of the SnS:Cu thin films.

Sample	E_g (eV)	Thickness (nm)
SnS:Cu (0%)	3.51	150.9
SnS:Cu (2%)	1.82	100.5
SnS:Cu (5%)	2.16	75.8
SnS:Cu (10%)	2.20	42.1

From Table 4, we can see how the value of E_g exceeds 1.72 eV, which is a value reported for thin SnS films with a cubic crystalline structure [31,38]. The increase of E_g was noted

with the doping percentage once the doping agent Cu is active. This behavior may be attributed to the change of lattice parameters inside the crystalline nature of the doping agent (cubic structure). The SnS film E_g with orthorhombic structure is the highest with the value of 3.51 eV, a higher bandgap value than what the literature recommends. This may be due to the structural phases of the film interfering with the expected transmittance of the SnS semiconductor. In addition, the lack of crystallinity and the thickness of the doped films may influence the obtained E_g causing it to increase, as samples reported in [34].

3.5. Electrical Properties

In Figure 7, mobility, carrier concentration, and resistivity obtained by the Hall–Van der Pauw technique are shown as a function of the copper concentration of SnS:Cu thin films [22]. All of the films are found to exhibit p-type natures, indicated by a positive Hall voltage. On increasing the doping concentration, parameters like carrier concentration and hole mobility tend to increase. For the particular case of mobility, grain boundaries act as scattering centers, then, due to small crystallite distributed randomly, carriers have to travel multiple grain boundaries, resulting in low mobility. Then, it is likely that a better distribution of small crystallite, in the deposited films, is the main reason for the increase in mobility of charge carriers. Therefore, films with greater homogeneity on crystallite distribution can show more mobility with respect to films with lesser homogeneity. The results of GLCM from SEM investigation, in Table 3, can confirm the influence of homogeneity on mobility.
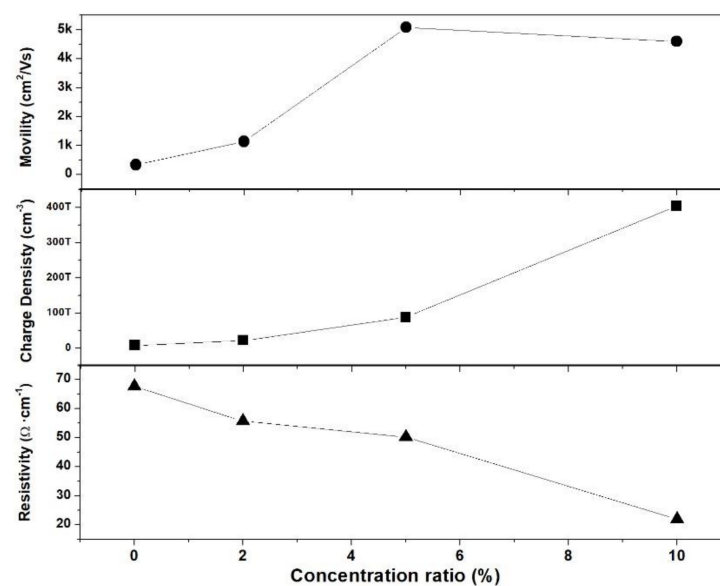
Figure 7. Electrical properties (mobility, charge density, and resistivity) of SnS:Cu thin films [22]. Copyright permission from: IEEE.

The resistivity of undoped SnS films is the highest, probably due to smaller grain size or the presence of voids or defects existing in the layers. Consequently, the resistivity decreases as the doping percentage of the films increases. This behavior has been detected in other work [9] for the same doping agent Cu and other elements like In and Sb [5,39]. This reduction in resistivity could be attributed to the excess charge created by an increased Sn/S atomic percent ratio. Ionized tin vacancies (Sn^{++}) are responsible for the p-type conductivity in SnS thin films [40]. Then, the presence of Cu atoms in form of impurities or charge neutralizer in the SnS structure increases the acceptor states. This is supported by the increase in the p-type carrier concentration observed in the same Figure 7.

Due to values found of high absorption coefficient and a better conductivity than the SnS, SnS:Cu could have the potential as a possible absorber layer in a solar cell. In this case,

SCAPS software was used to simulate the SnS:Cu-based solar cell and validate the physical parameters of the material as an absorber layer.

3.6. Results of SCAPS Simulation

Due to specific optoelectronic characteristics required to an absorbent layer in a solar cell and based on experimental results of the SnS:Cu from this work, this subsection considers comparing the results of the device proposed and simulated using the properties of each SnS:Cu thin film as an absorbent layer excluding the undoped thin film $y = 0\%$ due to the consideration of these films causing convergence errors within the SCAPS program, mainly due to their high E_g value. The properties of the other layers are based on the parameters reported by Mimbashi et al. as well as some of the parameters of the Cu-doped layers [27]. It is worth mentioning that the parameters were optimized since the properties of the material can differ if deposited by different techniques. Minbashi et al. implement the glancing angle deposition (GLAD) technique whereas, in this work, the USP technique was used. To investigate the effect of the absorbent layer, simulations were performed on the structures shown in Figure 2. As already mentioned in Section 2.4, the properties of SnS:Cu with concentration rates of $y = 2\%$, 5%, and 10% obtained will be simulated for its use as an absorbent layer in a structure. Table 5 shows the main properties of the absorbent layers used for the simulation by SCAPS.

Table 5. Main parameters for the different concentrations for Cu-doped SnS as absorbent layers.

Parameters and Units	Simulated Layers		
	$y = 2\%$	$y = 5\%$	$y = 10\%$
Thickness (nm)	100.5	75.8	42.1
bandgap (eV)	1.82	2.16	2.2
electron affinity (eV)	3.87	3.87	3.87
dielectric permittivity (relative)	12.5	12.5	12.5
CB effective density of states $(1/cm^3)$ [27]	7.5×10^{18}	7.5×10^{18}	$7.5\ 10^{18}$
VB effective density of states $(1/cm^3)$ [27]	1×10^{19}	1×10^{19}	1×10^{19}
electron thermal velocity (cm/s)	1×10^7	1×10^7	1×10^7
hole thermal velocity (cm/s)	1×10^7	1×10^7	1×10^7
electron mobility $(cm^2/V\ s)$ [27]	100	100	100
hole mobility $(cm^2/V\ s)$	1140	5083	4600

Figure 8 shows J–V curves obtained from SCAPS using the values of Table 5. The simulation was carried out at a working temperature of 300 K and under one sun (AM1.5G, 1000 W/m^2) spectra irradiation. The optimized solar cell parameters for the Cu-doped SnS absorbent layer are summarized in Table 6.
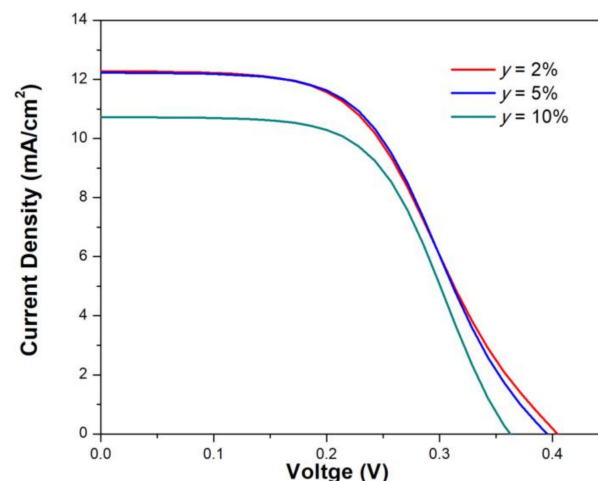
Figure 8. J–V curves of simulated layers SnS:Cu (2%, 5%, 10%).

Table 6. Functional parameters V_{oc}, J_{sc}, FF and Efficiency of Simulated SnS:Cu layer in solar cell.

Simulated Layer	V_{oc} (V)	J_{sc} (mA/cm^2)	FF (%)	η (%)
SnS:Cu (2%)	0.4043	12.282437	49.77	6.18
SnS:Cu (5%)	0.3951	12.231536	51.88	6.27
SnS:Cu (10%)	0.3621	10.723841	57.80	5.61

In Figure 8, it is possible to observe differences in the curves J–V for each y value, indicating the impact of Cu-concentration on SnS as an absorbent layer into a solar cell structure. Functional parameters such as open-circuit voltage (V_{oc}), short-circuit current density (J_{sc}), filling factor (FF), and efficiency (η) contained in Table 6 show an increase up to $y = 5\%$ in the sample. This behavior may be due to the increase in absorption coefficient and the mobility on type-p charges observed in Section 3.5 and their effect inside the simulated solar cell. The case of the observed drop in these parameters of the $y = 10\%$ sample would probably be due to the effect of low thickness shown in Table 4. The thickness absorber plays a significant part in solar cell performance. The thickness of the absorbent layer mainly controls the generation of photo-generated carriers [41]. It may be possible to further enhance device efficiency by increasing the SnS:Cu absorber layer thickness.

The effect of thickness on solar cell performance was observed through simulations for the Cu-doped SnS thin layers. Figure 9 and Table 7 show the η values of the devices considering only variants in the thickness from 0.1 to 1 µm in slopes of 100 nm for the absorbent layers of the Solar cell, where all other parameters stayed the same.
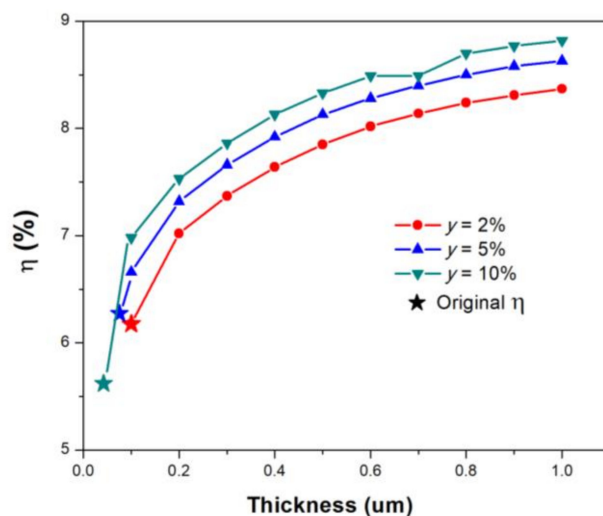
Figure 9. Thickness effect in the absorbent layer SnS:Cu.

Table 7. Thickness effect in the absorbent layer SnS:Cu.

Thickness of the Absorbent Layers (µm)	Efficiency of the Solar Cell		
	$y = 2\%$	$y = 5\%$	$y = 10\%$
0.1	6.18	6.66	6.98
0.2	7.02	7.32	7.53
0.3	7.37	7.66	7.86
0.4	7.64	7.92	8.13
0.5	7.85	8.13	8.33
0.6	8.02	8.28	8.49
0.7	8.14	8.4	8.49
0.8	8.24	8.5	8.7
0.9	8.31	8.58	8.77
1	8.37	8.63	8.82

As shown in Figure 9 and Table 7, the increase in the thickness of the SnS:Cu layer provokes efficiency rises of the simulated solar cell for all cases. This can be because an absorbing layer with a higher thickness allows more photons to be absorbed and increases the probability for more electric-generated carriers. The increment of this parameter can lead to optimal performance of the solar cell since the photogenerated currents along with the absorbed photons for longer wavelengths increase, propitiating a better J_{sc} and V_{oc} [41].

4. Conclusions

Thin films of SnS:Cu at concentrations ratio of 0%, 2%, 5%, and 10% were obtained by the USP technique, and the effect of the dopant agent on the structural, morphological, optical, and electrical properties were analyzed. These properties were considered to simulate a solar cell using SnS:Cu as an absorbent layer with the SCAPS program.

The structural analysis showed a change in the crystalline structure of the unit cell with the introduction of Cu as a dopant agent. The EDS study indicates the presence of Cu in all doped samples denoting a more percentage with the increase of y, as to be expected. As an original contribution to this studio, textural features based on the method of grey level co-occurrence matrix applied to Images of SEM were used to discuss the morphological properties of the samples. By this image analysis, SnS:Cu (10%) sample presented the lower homogeneity and higher correlation of all samples, which indicates a better distribution of the Cu element in the thin film surface with the increasing of y.

The Tauc method was employed using the transmittance and reflectance obtained by UV-Vis spectroscopy. The γ value was better adjusted to indicate that allowed indirect optical transitions correspond to the nature of the thin films. The method reveals an increment of the E_g as y does for the doped samples, and this may be due to the Cu atoms interfering with the absorption properties of the SnS that would agree with the shift in the lattice parameters for structural properties. The electrical study of the material shows a p-type nature for all the samples and an electrical improvement as the doping concentration increases. This means a higher concentration of the charges as well as better mobility associated with the homogeneity of the samples. In the same way, the reduction in resistivity is notable and could be attributed to the excess charge created by an increased Sn/S atomic percent ratio.

With a higher absorption coefficient and low resistivity found in the deposited material, Cu-doped SnS films are discussed as an alternative for an absorbent layer in solar cell devices. Using parameters reported by Mimbashi et al., an SnS:Cu-based solar cell was proposed and simulated by SCAPS. From the J–V curves produced by the program, it was possible to observe that the characteristics caused by doping in the absorbent layer generate better values in the fundamental parameters V_{oc}, J_{sc}, *FF,* and η. It should be noted that increasing the thickness in the absorbent layer can increase the efficiency value as discussed. The optimization of the parameters obtained in this work supports the fabrication possibility of high-efficiency photovoltaic devices. Being able to manufacture solar cells based on SnS:Cu thin films as an absorbing layer has an advantage, as it is a material obtained employing a relatively economic technique.

Author Contributions: Conceptualization, C.Á.-M. and S.R.-C.; methodology, S.R.-C. and B.R.-D.; software, L.S.-C.; validation, M.R., R.L.-P. and L.S.-C.; formal analysis, C.Á.-M.; investigation, C.Á.-M. and S.R.-C.; data curation, B.R.-D. and J.N.-R.; writing—original draft preparation, S.R.-C.; writing—review and editing, C.Á.-M., M.R., R.L.-P. and L.S.-C.; visualization, M.R. and L.S.-C.; supervision, C.Á.-M. and M.R.; project administration, C.Á.-M. All authors have read and agreed to the published version of the manuscript.

Funding: This research received no external funding.

Institutional Review Board Statement: Not applicable.

Informed Consent Statement: Not applicable.

Data Availability Statement: Not applicable.

Acknowledgments: The authors are thankful to TecNM for the financial support. Thanks to Patricia Altuzar for XRD diffractograms (Project LYFICS-CONACYT No. 132122), to Francisco Alvarado and Velumani Subramaniam for SEM and EDS studies (SENER-CONACYT No. 263043), to Aaron Sanchez for the use of the Spray Pyrolysis Laboratory and Karunakaran Nair for his support during the research stay. Sergio Rodriguez and Bernardo Reyes want to thank CONACYT for the scholarship with CVU numbers 740722 and 949051, respectively. We thank Proffesor Marc Burgelman for the SCAPS installation information.

Conflicts of Interest: The authors declare no conflict of interest.

Abbreviations

List of Symbols
Greek Letters

λ	Wavelength (nm)
θ	Angle Position (°)
α	Absorption coefficient (cm^{-1})
γ	Electronic transition nature
η	Solar cell efficiency (%)

Nomenclature

y	Doping concentration (%)
M	Molarity (mol/L)
d_{hkl}	Interplanar distance (nm)
h	Miller Index h
k	Miller Index k
l	Miller Index l
a	Lattice parameter a (nm)
b	Lattice parameter b (nm)
c	Lattice parameter c (nm)
d	Thin film thickness (nm)
R	Optical Reflectance (%)
T	Optical transmittance (%)
$h\nu$	Photon Energy (eV)
E_g	Optical band gap (eV)
B	Tauc constant
FF	Filling Factor (%)

Subscripts

oc	Open circuit
sc	Short circuit

References

1. Aghaei, M. A Review on Comparison between Traditional Silicon Solar Cells and Thin-Film CdTe Solar Cells. In Proceedings of the National Graduate Conference 2012 (NatGrad2012), Kajang, Malaysia, 8–10 November 2012; pp. 967–978.
2. Reddy, N.K.; Devika, M.; Gopal, E.S.R. Review on Tin (II) Sulfide (SnS) material: Synthesis, properties, and applications. *Crit. Rev. Solid State Mater. Sci.* **2015**, *40*, 359–398. [CrossRef]
3. Qu, Z.; Wang, L.; Tang, H.; Ye, H.; Li, M. Effect of Nano-SnS and Nano-MoS$_2$ on the corrosion protection performance of the polyvinylbutyral and zinc-rich polyvinylbutyral coatings. *Nanomaterials* **2019**, *9*, 956. [CrossRef]
4. Ge, Y.-H.; Guo, Y.-Y.; Shi, W.-M.; Qiu, Y.-H.; Wei, G.-P. Influence of in-doping on resistivity of chemical bath deposited SnS films. *J. Shanghai Univ.* **2007**, *11*, 403–406. [CrossRef]
5. Chaki, S.H.; Chaudhary, M.D.; Deshpande, M. Effect of indium and antimony doping in SnS single crystals. *Mater. Res. Bull.* **2015**, *63*, 173–180. [CrossRef]
6. Ninan, G.G.; Rajeshmon, V.G.; Kartha, C.S.; Vijayakumar, K.P. Cu doping: An effective method for improving optoelectronic properties of sprayed SnS thin films. In *AIP Conference Proceedings*; American Institute of Physics: College Park, MD, USA, 2014; Volume 1591, pp. 1440–1442.
7. Silvestre, S.; Kichou, S.; Guglielminotti, L.; Nofuentes, G.; Alonso-Abella, M. Degradation analysis of thin film photovoltaic modules under outdoor long term exposure in Spanish continental climate conditions. *Sol. Energy* **2016**, *139*, 599–607. [CrossRef]
8. Demtsu, S.; Albin, D.; Sites, J. Role of Copper in the Performance of CdS/CdTe Solar Cells. In Proceedings of the 2006 IEEE 4th World Conference on Photovoltaic Energy Conference, Waikoloa, HI, USA, 7–12 May 2006; Volume 1, pp. 523–526.

9.   Bommireddy, P.R.; Musalikunta, C.S.; Uppala, C.; Park, S.-H. Influence of Cu doping on physical properties of sol-gel processed SnS thin films. *Mater. Sci. Semicond. Process.* **2017**, *71*, 139–144. [CrossRef]

10.   Akkari, A.; Reghima, M.; Guasch, C.; Kamoun-Turki, N. Effect of copper doping on physical properties of nanocrystallized SnS zinc blend thin films grown by chemical bath deposition. *J. Mater. Sci.* **2012**, *47*, 1365–1371. [CrossRef]

11.   Tanusevski, A. Optical and photoelectric properties of SnS thin films prepared by chemical bath deposition. *Semicond. Sci. Technol.* **2003**, *18*, 501–505. [CrossRef]

12.   Gao, C.; Shen, H.; Sun, L.; Shen, Z. Chemical bath deposition of SnS films with different crystal structures. *Mater. Lett.* **2011**, *65*, 1413–1415. [CrossRef]

13.   Gedi, S.; Reddy, V.R.M.; Alhammadi, S.; Moon, D.; Seo, Y.; Kotte, T.R.R.; Park, C.; Kim, W.K. Effect of thioacetamide concentration on the preparation of single-phase SnS and SnS2 thin films for optoelectronic applications. *Coatings* **2019**, *9*, 632. [CrossRef]

14.   Son, S.-I.; Shin, D.; Son, Y.G.; Son, C.S.; Kim, D.R.; Park, J.H.; Kim, S.; Hwang, D.; Song, P. Effect of working pressure on the properties of RF sputtered SnS thin films and photovoltaic performance of SnS-based solar cells. *J. Alloys Compd.* **2020**, *831*, 154626. [CrossRef]

15.   Arepalli, V.K.; Shin, Y.; Kim, J. Photovoltaic behavior of the room temperature grown RF-Sputtered SnS thin films. *Opt. Mater.* **2019**, *88*, 594–600. [CrossRef]

16.   Di Mare, S.; Menossi, D.; Salavei, A.; Artegiani, E.; Piccinelli, F.; Kumar, A.; Mariotto, G.; Romeo, A. SnS thin film solar cells: Perspectives and limitations. *Coatings* **2017**, *7*, 34. [CrossRef]

17.   Sajeesh, T.; Warrier, A.R.; Kartha, C.S.; Vijayakumar, K. Optimization of parameters of chemical spray pyrolysis technique to get n and p-type layers of SnS. *Thin Solid Films* **2010**, *518*, 4370–4374. [CrossRef]

18.   Sajeesh, T.H.; Jinesh, K.B.; Rao, M.; Kartha, C.S.; Vijayakumar, K.P. Defect levels in SnS thin films prepared using chemical spray pyrolysis. *Phys. Status Solidi* **2012**, *209*, 1274–1278. [CrossRef]

19.   Patil, P.S. Versatility of chemical spray pyrolysis technique. *Mater. Chem. Phys.* **1999**, *59*, 185–198. [CrossRef]

20.   Decock, K.; Khelifi, S.; Burgelman, M. Modelling multivalent defects in thin film solar cells. *Thin Solid Films* **2011**, *519*, 7481–7484. [CrossRef]

21.   Niemegeers, A.; Burgelman, M.; Decock, K.; Degrave, S.; Verschraegen, J. Simulation Programme SCAPS-1D for Thin Film Solar Cells Developed at ELIS, University of Gent. Available online: https://scaps.elis.ugent.be/ (accessed on 24 May 2021).

22.   Rodriguez-Castro, S.; Rios, J.N.; Escalante, G.; Santana, G.; Sanchez-Juarez, A.; Álvarez-Macías, C. Deposition and characterization of SnS:Cu thin films by ultrasonic spray pyrolysis technique to applications in photovoltaic devices. In Proceedings of the 2018 IEEE 7th World Conference on Photovoltaic Energy Conversion (WCPEC) (A Joint Conference of 45th IEEE PVSC, 28th PVSEC & 34th EU PVSEC), Waikoloa, HI, USA, 10–15 June 2018; pp. 3305–3308.

23.   Herrera, N.; Orozco, S.; Rivero, M.; Loera, R.; Alvarez, C. Effect of asynchronous data processing on solar irradiance and clearness index estimation by sky imagery. *Appl. Sol. Energy* **2020**, *56*, 508–516. [CrossRef]

24.   Haralick, R.M.; Shanmugam, K.; Dinstein, I. Textural features for image classification. *IEEE Trans. Syst. Man Cybern.* **1973**, *SMC-3*, 610–621. [CrossRef]

25.   Burgelman, M.; Decock, K.; Khelifi, S.; Abass, A. Advanced electrical simulation of thin film solar cells. *Thin Solid Films* **2013**, *535*, 296–301. [CrossRef]

26.   Nykyruy, L.; Yavorskyi, R.; Zapukhlyak, Z.; Wisz, G.; Potera, P. Evaluation of CdS/CdTe thin film solar cells: SCAPS thickness simulation and analysis of optical properties. *Opt. Mater.* **2019**, *92*, 319–329. [CrossRef]

27.   Minbashi, M.; Ghobadi, A.; Ehsani, M.; Dizaji, H.R.; Memarian, N. Simulation of high efficiency SnS-based solar cells with SCAPS. *Sol. Energy* **2018**, *176*, 520–525. [CrossRef]

28.   Sinsermsuksakul, P.; Sun, L.; Lee, S.W.; Park, H.; Kim, S.B.; Yang, C.; Gordon, R.G. Overcoming efficiency limitations of sns-based solar cells. *Adv. Energy Mater.* **2014**, *4*, 1400496. [CrossRef]

29.   Calixto-Rodriguez, M.; Martinez, H.; Sanchez-Juarez, A.; Campos-Alvarez, J.; Tiburcio-Silver, A.; Calixto, M.E. Structural, optical, and electrical properties of tin sulfide thin films grown by spray pyrolysis. *Thin Solid Films* **2009**, *517*, 2497–2499. [CrossRef]

30.   Garcia-Angelmo, A.R.; Nair, M.; Nair, P. Evolution of crystalline structure in SnS thin films prepared by chemical deposition. *Solid State Sci.* **2014**, *30*, 26–35. [CrossRef]

31.   Nair, P.K.; Garcia-Angelmo, A.R.; Nair, M.T.S. Cubic and orthorhombic SnS thin-film absorbers for tin sulfide solar cells. *Phys. Status Solidi* **2015**, *213*, 170–177. [CrossRef]

32.   Donland, R.A. *Ciencia e Ingeniería de los Materiales*; Thomson-Paraninfo: Madrid, Spain, 2001.

33.   Baby, B.H.; Mohan, D.B. Co-sputtering Deposition of Cu Doped SnS Thin Films for Photovoltaic Application: Phase Stability, Microstructure and Optical Properties. In *AIP Conference Proceedings*; AIP Publishing LLC: Melville, NY, USA, 2017; Volume 1849, p. 020001. [CrossRef]

34.   Sebastian, S.; Kulandaisamy, I.; Arulanantham, A.M.S.; Valanarasu, S.; Kathalingam, A.; Jebathew, A.J.; Shkir, M.; Karunakaran, M. Influence of Al doping concentration on the opto-electronic chattels of SnS thin films readied by NSP. *Opt. Quantum Electron.* **2019**, *51*, 100. [CrossRef]

35.   Wang, Y.; Capretti, A.; Negro, L.D. Wide tuning of the optical and structural properties of alternative plasmonic materials. *Opt. Mater. Express* **2015**, *5*, 2415–2430. [CrossRef]

36. Fadavieslam, M.R.; Shahtahmasebi, N.; Rezaee-Roknabadi, M.; Bagheri-Mohagheghi, M.M. A study of the photoconductivity and thermoelectric properties of SnxSyoptical semiconductor thin films deposited by the spray pyrolysis technique. *Phys. Scr.* **2011**, *84*, 035705. [CrossRef]

37. Salah, H.B.H.; Bouzouita, H.; Rezig, B. Preparation and characterization of tin sulphide thin films by a spray pyrolysis technique. *Thin Solid Films* **2005**, *480–481*, 439–442. [CrossRef]

38. Garcia-Angelmo, A.R.; Romano-Trujillo, R.; Campos-Álvarez, J.; Gomez-Daza, O.; Nair, M.T.S.; Nair, P.K. Thin film solar cell of SnS absorber with cubic crystalline structure. *Phys. Status Solidi* **2015**, *212*, 2332–2340. [CrossRef]

39. Urbaniak, A.; Pawłowski, M.; Marzantowicz, M.; Sall, T.; Marí, B. Opto-electrical characterisation of In-doped SnS thin films for photovoltaic applications. *Thin Solid Films* **2017**, *636*, 158–163. [CrossRef]

40. Hegde, S.; Kunjomana, A.; Murahari, P.; Prasad, B.; Ramesh, K. Vacuum annealed tin sulfide (SnS) thin films for solar cell applications. *Surf. Interfaces* **2018**, *10*, 78–84. [CrossRef]

41. Karthick, S.; Velumani, S.; Bouclé, J. Experimental and SCAPS simulated formamidinium perovskite solar cells: A comparison of device performance. *Sol. Energy* **2020**, *205*, 349–357. [CrossRef]